

The dispersion of spherical droplets in source–sink flows and their relevance to the COVID-19 pandemic


Cite as: Phys. Fluids **32**, 083302 (2020); <https://doi.org/10.1063/5.0021427>

Submitted: 10 July 2020 • Accepted: 21 July 2020 • Published Online: 04 August 2020

 C. P. Cummins,  O. J. Ajayi,  F. V. Mehendale, et al.

COLLECTIONS

Paper published as part of the special topic on [Flow and the Virus](#)

 This paper was selected as Featured



View Online



Export Citation



CrossMark

ARTICLES YOU MAY BE INTERESTED IN

[Can a toilet promote virus transmission? From a fluid dynamics perspective](#)

Physics of Fluids **32**, 065107 (2020); <https://doi.org/10.1063/5.0013318>

[A mathematical framework for estimating risk of airborne transmission of COVID-19 with application to face mask use and social distancing](#)

Physics of Fluids **32**, 101903 (2020); <https://doi.org/10.1063/5.0025476>

[Virus transmission from urinals](#)

Physics of Fluids **32**, 081703 (2020); <https://doi.org/10.1063/5.0021450>

APL Machine Learning

Open, quality research for the networking communities

Now Open for Submissions

LEARN MORE

The dispersion of spherical droplets in source–sink flows and their relevance to the COVID-19 pandemic

Cite as: Phys. Fluids 32, 083302 (2020); doi: 10.1063/5.0021427

Submitted: 10 July 2020 • Accepted: 21 July 2020 •

Published Online: 4 August 2020



C. P. Cummins,^{1,2,a)}  O. J. Ajayi,¹  F. V. Mehendale,³  R. Gabl,⁴  and I. M. Viola⁴ 

AFFILIATIONS

¹Maxwell Institute for Mathematical Sciences, Department of Mathematics, Heriot-Watt University, Edinburgh EH14 4AS, United Kingdom

²Institute for Infrastructure and Environment, Heriot-Watt University, Edinburgh EH14 4AS, United Kingdom

³Centre for Global Health, Usher Institute, College of Medicine and Veterinary Medicine, University of Edinburgh, Edinburgh EH8 9AG, United Kingdom

⁴School of Engineering, University of Edinburgh, Edinburgh EH9 3FB, United Kingdom

Note: This paper is part of the Special Topic, Flow and the Virus.

a) Author to whom correspondence should be addressed: c.cummins@hw.ac.uk

ABSTRACT

In this paper, we investigate the dynamics of spherical droplets in the presence of a source–sink pair flow field. The dynamics of the droplets is governed by the Maxey–Riley equation with the Basset–Boussinesq history term neglected. We find that, in the absence of gravity, there are two distinct behaviors for the droplets: small droplets cannot go further than a specific distance, which we determine analytically, from the source before getting pulled into the sink. Larger droplets can travel further from the source before getting pulled into the sink by virtue of their larger inertia, and their maximum traveled distance is determined analytically. We investigate the effects of gravity, and we find that there are three distinct droplet behaviors categorized by their relative sizes: small, intermediate-sized, and large. Counterintuitively, we find that the droplets with a minimum horizontal range are neither small nor large, but of intermediate size. Furthermore, we show that in conditions of regular human respiration, these intermediate-sized droplets range in size from a few μm to a few hundred μm . The result that such droplets have a very short range could have important implications for the interpretation of existing data on droplet dispersion.

Published under license by AIP Publishing. <https://doi.org/10.1063/5.0021427>

I. INTRODUCTION

The transport of inertial particles in fluid flows occurs in many problems arising in engineering and biology, such as the build-up of microplastics in the ocean¹ and respiratory virus transmission through tract droplets.^{2–4} The Maxey–Riley equation⁵ describes the motion of a finite-sized spherical particle in an ambient fluid flow. The equation is a representation of Newton's second law in which the forces acting on the particle include a Stokesian drag force, an added mass force, a gravity force, the force due to the undisturbed flow, and a Basset–Boussinesq history term. The equation takes the form of a second-order, implicit integro-differential equation with a singular kernel and with a forcing term that is singular

at the starting time.⁶ The equation has been applied to model the dynamics of aerosol comprising particles of various density ratios,⁷ the feeding mechanism of jellyfish,^{8,9} and the dynamics of inertial particles in vortical flows.^{10–12} The equation has also been applied to droplet-laden flows with a phase change at sub-Kolmogorov scales.¹³

The Basset–Boussinesq term accounts for the drag due to the production of vorticity as the particle is accelerated from rest. It is difficult to include this term numerically and is often omitted on the assumption that particles move in a quasistatic manner.¹⁴ This assumption breaks down in bubbly and slurry flows, where the Basset–Boussinesq term accounts for a quarter of the forces on the particle¹⁴ when the density ratio $R = 2\rho_f' / (\rho_f' + 2\rho_p')$ is greater than $2/3$, where ρ_f' is the fluid density and ρ_p' is the particle density. Recent

advances¹⁵ have shown that the full Maxey–Riley equation can be represented as a forced, time-dependent Robin boundary condition of the 1D diffusion equation. Here, the authors found that a particle settling under gravity relaxes to its terminal velocity according to $t^{-1/2}$; however, if the Basset–Boussinesq term is neglected, it relaxes exponentially quickly.¹⁶

In this paper, we examine the transport of inertial particles in source–sink flows.¹⁷ Such a flow could represent the trajectories of water droplets emitted from coughing, sneezing,^{2–4} or breathing and in the presence of extraction, such as an air-conditioning unit or air current.¹⁸ Our simplified mathematical model yields to analytic treatment in certain limits of large and small droplets. This enables us to provide important physical insight into this complex problem, but we remark that the effects such as drag non-linearity¹⁹ and turbulent dispersion²⁰ are not taken into account. Since the dynamics of settling droplets is significantly affected by their size, it is important to understand the impact that the emitted droplet size has on the destination of such a droplet in a source–sink flow. In particular, since droplets are vectors for infectious diseases such as COVID-19, it is imperative that we understand the droplet dynamics in such flows to mitigate the spread of the disease.

This paper is organized as follows: in Sec. II, the mathematical model is presented and non-dimensionalized. The results are presented in Sec. III for small (Sec. III A) and intermediate-sized (Sec. III B) droplets in the absence of gravity. Gravitational effects are considered for small droplets in Sec. III C and for intermediate-sized droplets in Sec. III D. In Sec. IV, we present applications of our results for human breathing without (Sec. IV B) and with (Sec. IV C) the inclusion of extraction. Finally, we discuss our findings in Sec. V.

II. MATHEMATICAL MODEL

Consider a source producing air of density ρ'_{air} and viscosity ν'_{air} , with volume flux of Q'_1 , containing spherical liquid droplets of density ρ'_{drop} , which are emitted with a characteristic velocity U' . Let us represent the 3D velocity field $\mathbf{u}'_{\text{source}}(\mathbf{x}')$ at a position \mathbf{x}' of the emitted air as a point source of strength Q'_1 , centered at the origin in the Cartesian coordinates,¹⁷

$$\mathbf{u}'_{\text{source}}(\mathbf{x}') = \frac{Q'_1 \mathbf{x}'}{4\pi |\mathbf{x}'|^3}. \quad (1)$$

We include an extraction unit as a point sink of strength Q'_2 located at a position \mathbf{x}'_0 as follows:

$$\mathbf{u}'_{\text{sink}}(\mathbf{x}') = -\frac{Q'_2(\mathbf{x}' - \mathbf{x}'_0)}{4\pi |\mathbf{x}' - \mathbf{x}'_0|^3}. \quad (2)$$

The resulting airflow is given by the linear superposition of these two flows,

$$\mathbf{u}'(\mathbf{x}') = \frac{Q'_1 \mathbf{x}'}{4\pi |\mathbf{x}'|^3} - \frac{Q'_2(\mathbf{x}' - \mathbf{x}'_0)}{4\pi |\mathbf{x}' - \mathbf{x}'_0|^3}. \quad (3)$$

The natural timescale of the problem emerges as $T' = |\mathbf{x}'_0|/U'$. We non-dimensionalize (3) according to

$$\mathbf{x} = \mathbf{x}'/|\mathbf{x}'_0| \quad \mathbf{u} = \mathbf{u}'/U', \quad (4)$$

which gives the non-dimensionalized expression for the airflow velocity

$$\mathbf{u}(\mathbf{x}) = \Lambda \left(\frac{\mathbf{x}}{|\mathbf{x}|^3} - \gamma \frac{(\mathbf{x} - \mathbf{x}_0)}{|\mathbf{x} - \mathbf{x}_0|^3} \right), \quad (5)$$

with $\Lambda = Q'_1/4\pi U'|\mathbf{x}'_0|^2$, $\gamma = Q'_2/Q'_1$, and $\mathbf{x}_0 = \mathbf{x}'_0/|\mathbf{x}'_0|$.

The velocity of the droplet embedded in this background airflow obeys the Maxey–Riley equation⁵

$$\begin{aligned} \dot{\mathbf{v}}(t) - \frac{3}{2}R \frac{D\mathbf{u}}{Dt} \Big|_{\mathbf{x}(t)} &= \left(1 - \frac{3}{2}R\right) \mathbf{g} - A(\mathbf{v}(t) - \mathbf{u}(\mathbf{X}(t), t)) \\ &\quad - \sqrt{\frac{9}{2\pi}} \frac{R}{\sqrt{St}} \left[\int_0^t \frac{\dot{\mathbf{v}}(s) - \dot{\mathbf{u}}(\mathbf{X}(s), s)}{\sqrt{t-s}} ds \right. \\ &\quad \left. + \frac{\mathbf{v}(0) - \mathbf{u}(\mathbf{X}(0), 0)}{\sqrt{t}} \right], \end{aligned} \quad (6)$$

where $\mathbf{X}(t)$ is the position of the droplet at time t , $\mathbf{v}(t) = \dot{\mathbf{X}}(t)$ is its velocity, the dot indicates the time derivative, and

$$\begin{aligned} R &= \frac{2\rho'_{\text{air}}}{\rho'_{\text{air}} + 2\rho'_{\text{drop}}}, \quad A = \frac{R}{St}, \\ St &= \frac{2}{9} \left(\frac{a'}{|\mathbf{x}'_0|} \right)^2 Re, \quad \mathbf{g} = \frac{|\mathbf{x}'_0| \mathbf{g}'}{U'^2}, \end{aligned} \quad (7)$$

with a' being the droplet radius, \mathbf{g}' being the acceleration due to gravity vector, $Re = U'|\mathbf{x}'_0|/\nu'_{\text{air}}$ is the Reynolds number, and St is the particle Stokes number. Note here that the Faxén correction terms⁵ have not been omitted: they are identically zero since $\Delta \mathbf{u} = \mathbf{0}$.

The approximate ratio of the Basset history drag to Stokes drag is $O(St^{1/2})$, which, for the range of St we are interested in, is generally much less than one. In the remainder of this paper, we neglect the Basset history term since we anticipate that its magnitude is negligible compared to the Stokes drag term for the parameters of interest to us, and the resulting equations are

$$\dot{\mathbf{v}}(t) - \frac{3}{2}R \frac{D\mathbf{u}}{Dt} \Big|_{\mathbf{x}(t)} = \left(1 - \frac{3}{2}R\right) \mathbf{g} - A(\mathbf{v}(t) - \mathbf{u}(\mathbf{X}(t), t)), \quad (8)$$

subject to the initial conditions $\mathbf{v}(0) = \mathbf{u}(\mathbf{X}(0), 0)$, where $\mathbf{X}(0)$ lie on a circle surrounding the origin of radius $|\mathbf{X}(0)|$. In (5), taking the limit

$$\lim_{\mathbf{x} \rightarrow 0} \mathbf{u}(\mathbf{x}) \simeq \frac{\Lambda \mathbf{X}}{|\mathbf{X}|^3}, \quad (9)$$

hence, we can ensure that the non-dimensional initial velocity has unit magnitude by requiring $|\mathbf{X}(0)| = \sqrt{\Lambda}$.

A. Computational considerations

The resulting equations (8) are a set of three coupled second-order non-linear ordinary differential equations (ODEs) for the position vector $\mathbf{X}(t)$. The algebra involved in computing the material derivative in (8) is straightforward, but cumbersome, and it is omitted here. This set of equations does not admit analytical solutions, in general, and so it must be solved numerically.

We solved the equations by expressing them as a system of six first-order ODEs using the MATLAB[®] ode15s algorithm, a variable-step, variable-order solver based on the numerical differentiation formulas.²¹ This was performed on a laptop equipped with

an Intel(R) Core(TM) i9-9980HK CPU (2.40 GHz) and 32 GB of RAM; each trajectory took on average 0.015 s to compute. In each of our plots, we show the trajectories emanating from 30 evenly spaced points on a circle centered at the origin (i.e., the source), giving a total simulation time of approximately 0.45 s. The number of trajectories was selected by balancing the requirements on the detail on individual trajectories and the global behavior of the droplets. Such short simulation times allow us to identify the most important combinations out of a wide range of variables in a computational time that is several orders of magnitude faster than models employing computational fluid dynamics.²²

III. THE RESULTS

A. Small droplets in the absence of gravity

In the absence of gravity, Eq. (8) reads (dropping the explicit time dependence)

$$\dot{\mathbf{v}} - \frac{3R}{2} [\mathbf{u} \cdot \nabla \mathbf{u}]_{\mathbf{X}} = -\frac{R}{St} (\mathbf{v} - \mathbf{u})_{\mathbf{X}}. \quad (10)$$

In (10), for small droplets ($St \ll R$) emitted from the source, the balance is between the first term on the left-hand side and the right-hand side so that the velocity rapidly adjusts to the background flow $\mathbf{v} \approx \mathbf{u}_{\mathbf{X}}$.

We are interested in whether droplets move away from or toward the sink. To this end, we look for trajectories for which $\mathbf{v} > 0$,

$$\mathbf{v} = \frac{d\mathbf{X}}{dt} > 0 \iff \frac{\mathbf{X}}{|\mathbf{X}|^3} > \gamma \frac{(\mathbf{X} - \mathbf{x}_0)}{|\mathbf{X} - \mathbf{x}_0|^3}. \quad (11)$$

If we take $\mathbf{x}_0 = [1, 0, 0]$, then the trajectory that emerges from the source and travels in the direction of the negative x -axis is the one that gets the greatest distance away from the sink. Hence, let us consider this inequality in the first component, and along the line $y = 0$, $z = 0$,

$$\frac{dX(t)}{dt} > 0 \iff \frac{X}{|X|^3} > \gamma \frac{(X-1)}{|X-1|^3}. \quad (12)$$

We are interested in where the flow field changes direction, since this indicates the maximum distance the droplets emitted at the source can travel before moving toward the sink. To this end, let us choose a point $x = -\lambda$ along $y = 0$ and $z = 0$; then, this inequality tells us that

$$\frac{dX(t)}{dt} > 0 \iff \gamma > \left(1 + \frac{1}{\lambda}\right)^2. \quad (13)$$

This inequality can hold only if $\gamma > 1$. This makes sense, since the flow is directed toward the sink only if the sink is stronger than the source.

Figure 1 shows the trajectories for small droplets ($St \ll R$) in the presence of a source–sink pair: the source is located at the origin (green disk) and the sink is located at $x = 1$ along the x -axis (red disk). For $\gamma = 1$ [Fig. 1(a)], we have equal strength and droplets can take large excursions from the source before returning to the sink. As γ increases, the trajectories emanating from the source occupy an increasingly compacted region [Figs. 1(b)–1(d)]. We can use this inequality above to define a region

$$|\lambda| < \frac{\sqrt{\gamma} + 1}{\gamma - 1} \quad (14)$$

such that small droplets do not get further than a distance $|\lambda|$ before traveling toward the sink. The circle with radius $|\lambda|$ is shown in Fig. 1 (dashed curve). Observe that, as one gets increasingly close to the source ($\lambda \rightarrow 0$), the inequality tends to

$$\frac{dX(t)}{dt} > 0 \iff \gamma > \frac{1}{\lambda^2}, \quad (15)$$

meaning that in order to maintain trajectories moving away from a given test point, the sink strength needs to increase quadratically with the distance of the test point to the source.

B. Intermediate-sized droplets in the absence of gravity

For $St = O(R)$ and $St \gg R$, the droplet is slowed down exponentially according to

$$\mathbf{v}(t) \approx \mathbf{v}(0) \exp[-(R/St)t], \quad (16)$$

which represents a balance between inertia and drag forces. Provided $\gamma > 1$, and in the absence of gravity, in the long-term, the droplet will always migrate toward the sink. However, in the case of intermediate-sized droplets, the maximum distance traveled by the droplet before it moves toward the sink is given by $|\mathbf{v}(0)|/(R/St)$. Since the initial velocity of the droplet is chosen to be the same as the surrounding fluid, then we can write the maximum distance as $|\mathbf{u}(\mathbf{X}(0), 0)|/(R/St)$. As explained above [see (9)], in our non-dimensionalization, our characteristic velocity U' was chosen to be that of the outlet. Hence, in this non-dimensionalization, $|\mathbf{u}(\mathbf{X}(0), 0)| = 1$.

Figure 2 shows the trajectories of intermediate-sized droplets for $\gamma = 5$ in the absence of gravity. The striking feature of the plot is the shift from a regime where the maximal extent of the trajectories as predicted by (14) is no longer valid and must be replaced with a circle of radius St/R . In Fig. 2(a), $St/R = 0.1$ so that the droplets are slowed down rapidly before following the fluid flow. In Fig. 2(b), $St/R = 1$, meaning that the droplets are slowed down over the area covered by the unit circle, before being brought to the sink as ideal tracers. Finally, in Fig. 2(c), $St/R = 2$ so that the droplets travel a non-dimensional distance of 2 before being slowed down enough to be pulled into the sink.

Hence, we find that, in the absence of gravity, we can have two very different behaviors depending on whether we have small droplets $St \ll R$ or intermediate-sized droplets $St \geq R$. Small droplets cannot get further than a distance $(\sqrt{\gamma} + 1)/(\gamma - 1)$ from the source before traveling toward the sink, but intermediate-sized droplets are not restricted by this and can travel further than this, provided $St/R > (\sqrt{\gamma} + 1)/(\gamma - 1)$.

C. The effect of gravity on small droplets

As the droplets move from the source to the sink, gravity attempts to pull them vertically downwards. Over the timescale of the problem, i.e., the average time it takes for a droplet to travel from the source to sink, gravity may or may not have an appreciable effect. Intuitively, one would imagine that smaller droplets are influenced more by the airflow than gravity: for stronger sinks, the effect of gravity is comparatively less. Intuitively, one would also expect that this holds true, provided that the source and sink are not too far away. The gravitational vector is non-dimensionalized according to

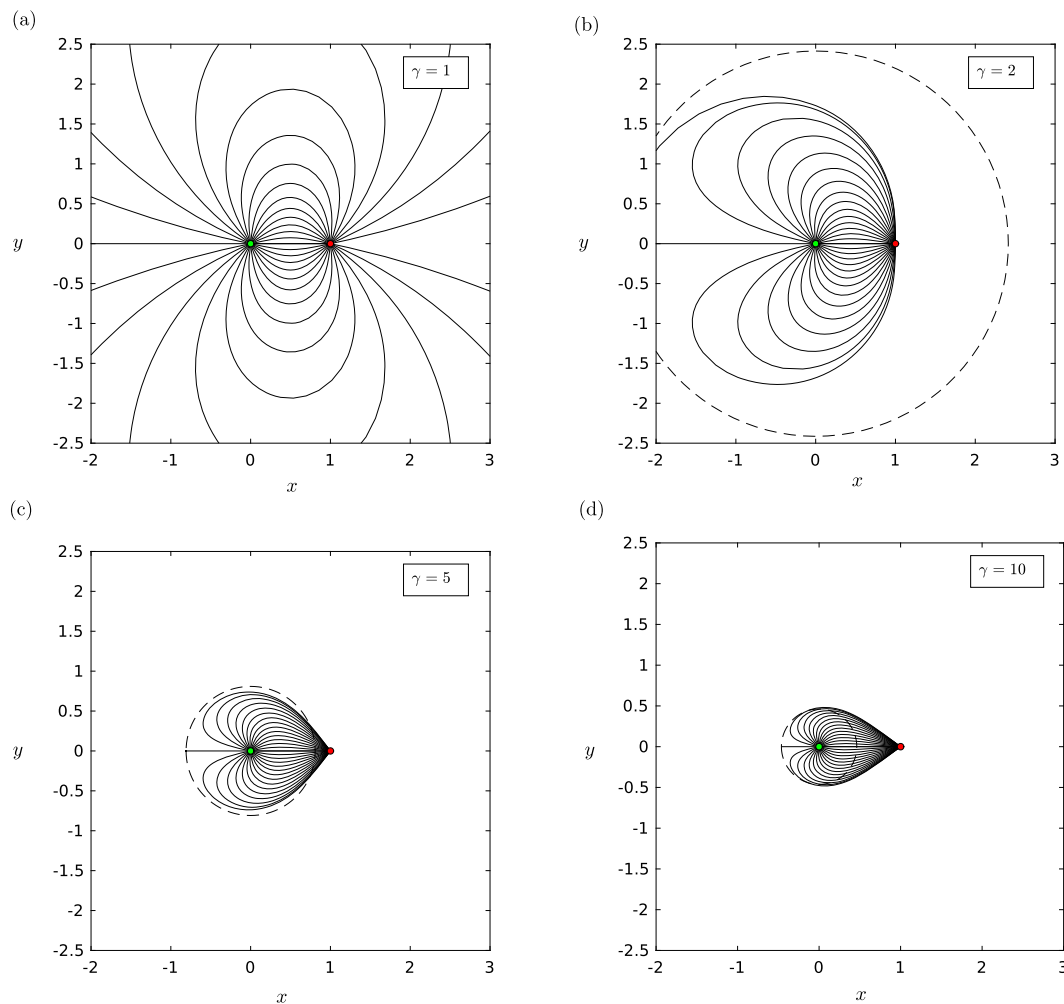


FIG. 1. The trajectories $\mathbf{X}(t)$ in the xy -plane of small droplets $St \ll R$ with a background source–sink pair of various strengths: (a) $\gamma = 1$, (b) $\gamma = 2$, (c) $\gamma = 5$, and (d) $\gamma = 10$. In these plots, $R = 0.001$, $\Lambda = 0.0001$, and $|\mathbf{g}| = 0$. The trajectories do not change for changing R . The dashed circle indicates the predicted maximal distance that a droplet can travel in this regime, calculated using the inequality (14). The source is indicated by a green filled circle, and the sink is indicated by a red filled circle.

$U'^2/|\mathbf{x}'_0|$ as shown in (7) so it depends on the initial speed and the distance between the source and sink.

For $St \ll R < 2/3$, and in the absence of gravity, there are three fixed points: the source, the sink, and a saddle point located at $x = -|\lambda|$ along the x -axis (Fig. 1). When gravitational effects are included, the fixed point at $x = -|\lambda|$ moves clockwise about the origin as the effect of gravity is increased [see Fig. 3(a)]. A fourth fixed point (saddle) is created far from the source–sink pair, which gradually moves toward the sink [Figs. 3(b) and 3(c)] as the effect of gravity is increased. In Fig. 3(d), the separatrices (indicated as the red dashed-dotted curves) show that there is a wedge of trajectories that escape the pull of the sink. As might be expected, these trajectories are those that point directly away from the sink. Our results show that even for small droplets, gravity can be important if either the sink is far away or if the ejection speed is too low.

D. The effect of gravity on intermediate-sized droplets

Small droplets are deflected by gravity but generally feel the pull of the sink. Whether or not they are pulled in is determined by the interaction of gravity, the angle of their trajectory, and γ . As the droplets become larger, gravitational effects dominate and the sink becomes ineffective. In Fig. 4, we show how the droplet trajectories behave as St is increased. Figure 4(a) shows the familiar situation where the droplets are so small that gravity does not appreciably affect their trajectory over the characteristic lengthscale.

As St is increased, Fig. 4(b) shows that there are a range of trajectories with ejection angles α (defined with respect to the positive sense of the x -axis) around the source, which are deflected downwards away from the sink. This is consistent with Sec. III C.

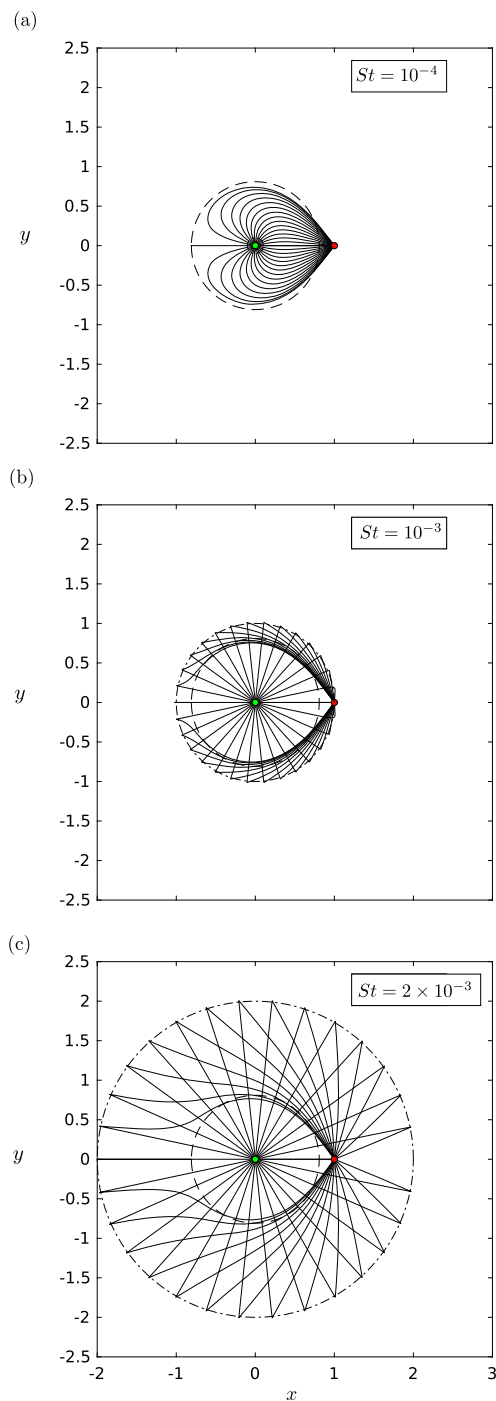


FIG. 2. The trajectories $\mathbf{X}(t)$ in the xy -plane of droplets with a background source–sink pair with strength ratio $\gamma = 5$ for various values of St : (a) $St = 10^{-4}$, (b) $St = 10^{-3}$, and (c) $St = 2 \times 10^{-3}$. In these plots, $R = 0.001$, $\Lambda = 0.0001$, and $|\mathbf{g}| = 0$. The dashed circle indicates the predicted maximal distance that a droplet can travel in this regime, calculated using the inequality (14). The dashed-dotted circle indicates the maximal distance predicted by the inertia–drag balance, giving radius equal to St/R . The source is indicated by a green filled circle and the sink is indicated by a red filled circle.

However, at a critical $St \approx 2.5 \times 10^{-6}$, each trajectory is deflected downwards by gravity [Fig. 4(c)]. In this case, the maximum horizontal distance traveled by the droplets is very small. Interestingly, this trend is not monotonic. Further increasing St , the trajectories adopt a ballistic trajectory [Fig. 4(d)]. Such droplets can move in very close proximity to the sink but are not pulled into it [Fig. 4(d)].

IV. EXAMPLES OF APPLICATION

A. Background on respiratory virus transmission

One of the possible applications of this paper is to underpin more sophisticated analytical or numerical models to study the transmission of respiratory viruses. In medical applications, it is common practice to categorize the emitted fluid particles as larger droplets from $5 \mu\text{m}$ to 1mm in diameter, which have a ballistic trajectory, and aerosol that remains airborne.²³ Droplets smaller than $5 \mu\text{m}$ and the desiccated droplet nuclei are known as aerosol, which can remain airborne for several hours.^{24–26} Respiratory viruses are transmitted from the virus-laden fluid particles to the recipient through (1) aerosol inhalation, (2) droplet deposition on the recipient’s mouth, nose, or conjunctiva, or (3) droplet deposition on a surface and successive transmission through physical contact.²⁷ The SARS-CoV-2 virus, for example, has a diameter of $70 \text{nm}–90 \text{nm}$,²⁸ and it is carried by droplets and aerosol.^{26,29}

The model proposed in this paper can provide new insights into the aerosol transmission, i.e., through those particles whose Stokes number is not sufficiently large to have a ballistic trajectory. The relative importance of aerosol (1) and droplet [(2) and (3)] virus transmission is not always known, and it is yet to be established for SARS-CoV-2.³⁰ Counterintuitively, it has been argued that aerosol could be more dangerous than larger droplets.³¹ Smaller droplets ($\leq 5 \mu\text{m}$) suspended in aerosol might carry a higher concentration of virus than larger droplets ($> 5 \mu\text{m}$).^{30,32,33} The largest droplets are less likely to penetrate deeply in the respiratory system and might be deactivated by the effective first structural and defense barrier of the mucosa.³⁴ Conversely, aerosolized virus half-life exceeds 1h ²⁶ and can be transported airborne through inhalation deep into the lungs,^{35–38} avoiding the defense mechanisms of the upper respiratory system. Furthermore, aerosol inoculation has been shown to cause more severe symptoms than droplets administered by intranasal inoculation, and the dose of influenza required for inoculation by the aerosol route is 2–3 orders of magnitude lower than the dose required by intranasal inoculation.^{2,33,38}

To apply our model to aerosol dispersion, we consider the particles ejected by a person talking. A person ejects about tens of fluid particles per second with diameters between³⁹ $0.1 \mu\text{m}$ to 1mm and with a speed of the order⁴⁰ of 1m s^{-1} . Because this is the most frequent source of aerosol, this accounts for most of the aerosol inhaled by other people.^{41,42} Coughing leads to the ejection of 100–1000 fluid particles per second with a speed around 10m s^{-1} , while sneezing generates 1000–10 000 fluid particles per second with a speed of up to⁴³ 20m s^{-1} . The values presented in this paragraph should be taken as indicative because there is a significant variability between different experimental studies.^{2,33,36,38,44–55}

Some of the physics that is not considered in this work is the particle–particle interaction and evaporation. In fact, fluid particles are ejected through a jet that transports particles in the range of

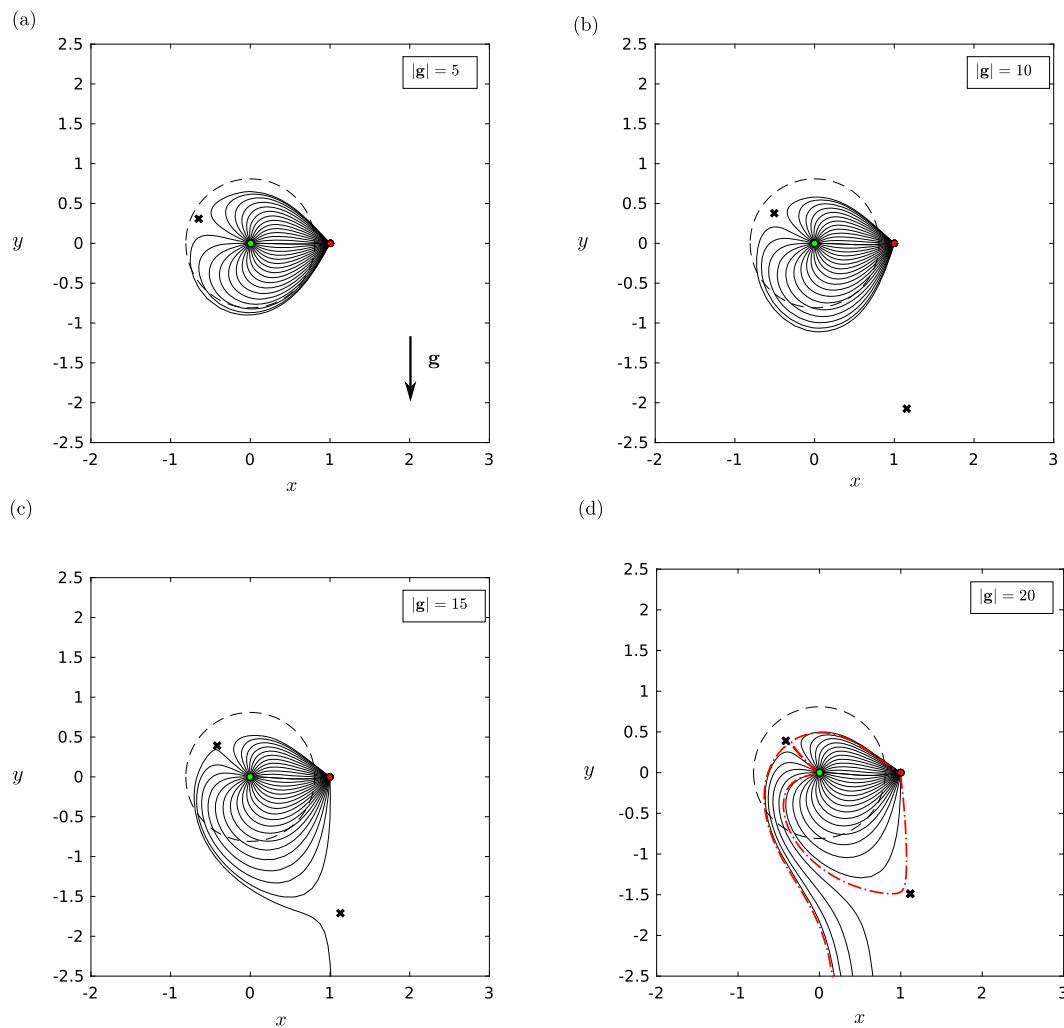


FIG. 3. The trajectories $\mathbf{X}(t)$ in the xy -plane of small droplets $St \ll R$ with a background source–sink pair with strength ratio $\gamma = 5$ and for various strengths of the gravity parameter: (a) $|g| = 5$, (b) $|g| = 10$, (c) $|g| = 15$, and (d) $|g| = 20$. In these plots, $R = 0.001$ and $\Lambda = 0.0001$. The trajectories will be different for different choices of R . The dashed circle indicates the predicted maximal distance that a fluid parcel can travel when ejected from the source. The black crosses indicate the position of saddle fixed points. The source is indicated by a green filled circle, and the sink is indicated by a red filled circle.

$2 \mu\text{m}$ – $150 \mu\text{m}$,^{45,56,57} i.e., the aerosol, while the largest droplets have a ballistic trajectory independent of the surrounding flow.^{2,57,58} The jet can be either laminar or turbulent when breathing and speaking, while coughing and sneezing always results in a turbulent jet with a diameter-based Reynolds number higher² than 10^4 . Once ejected, the air jet extends along a straight trajectory; its diameter increases linearly with the traveled distance, while the mean velocity linearly decreases, and the turbulent statistics remain constant (i.e., the jet is self similar⁵⁹). Once the largest particles with a ballistic trajectory have left the air jet, the jet bends upwards due to the buoyancy force caused by the temperature and thus density difference.² Smaller size particles ($\leq 100 \mu\text{m}$) are transported by the jet while they evaporate. Once a droplet exits the jet, it falls at its settling speed. For a particle with a diameter of $50 \mu\text{m}$ and $10 \mu\text{m}$, the settling speed

is less than 0.06 m s^{-1} and 0.03 m s^{-1} , respectively. The smallest of these two droplets is likely to land in the form of a desiccated nucleus. In fact, while a droplet with a diameter of $50 \mu\text{m}$ evaporates in about 6 s, a $10 \mu\text{m}$ droplet evaporates in less than^{2,60} 0.1 s, although their survivability also depends on the ambient temperature and relative humidity.²⁰ Once these droplets leave the jet, they can still be transported by ambient air currents, which have speeds typically in excess⁶¹ of 0.01 m s^{-1} . These currents are modeled by the sink–source flow field discussed in this paper.

A key issue that is discussed in this study is the extent to which the cloud of droplets and aerosol are displaced into the neighboring environment, as this is associated with virus transmission risk. Previous studies estimated that the overall horizontal range of the droplets generated while breathing and coughing before they land

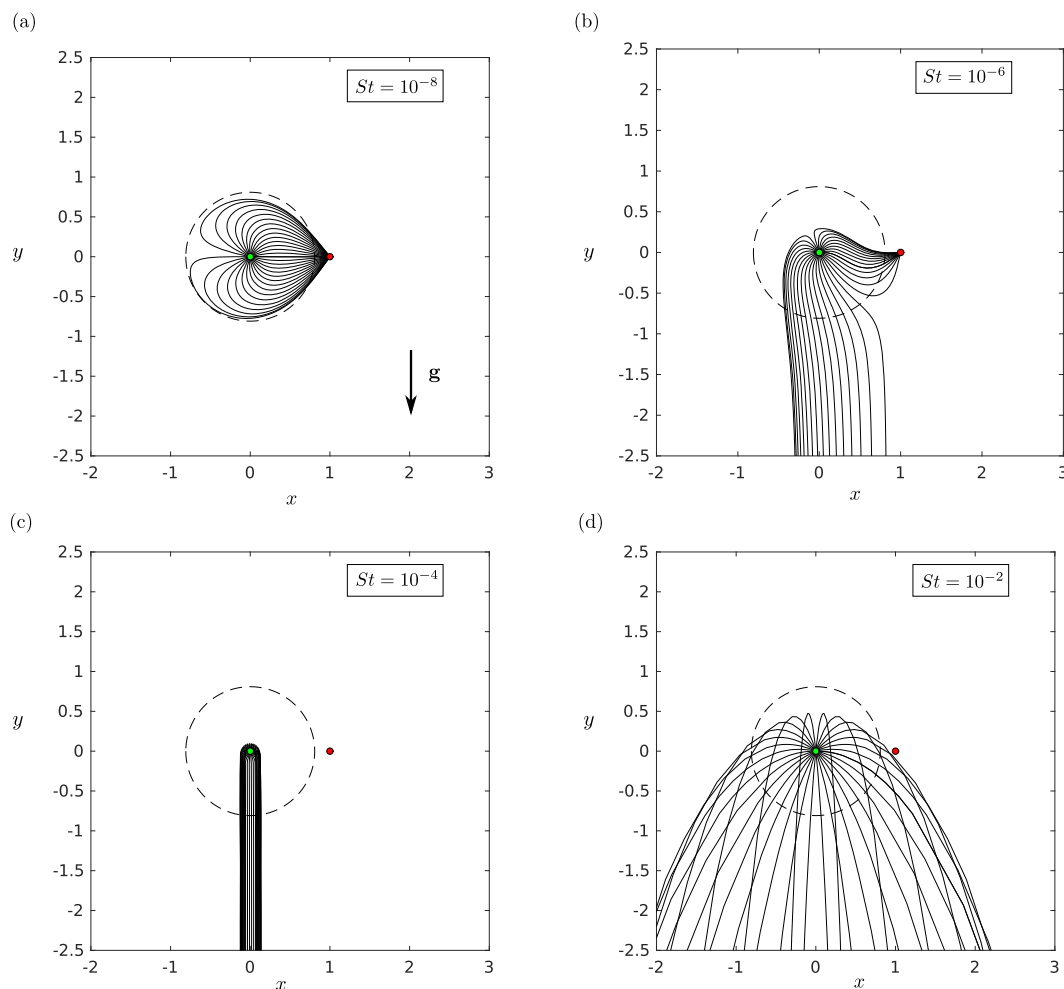


FIG. 4. The trajectories $\mathbf{X}(t)$ in the xy -plane with a background source–sink pair with strength ratio $\gamma = 5$ and for various Stokes numbers St : (a) $St = 10^{-8}$, (b) $St = 10^{-6}$, (c) $St = 10^{-4}$, and (d) $St = 10^{-2}$. In these plots, $R = 0.001$, $\Lambda = 0.0001$, and $|g| = 1$. The trajectories will be different for different choices of R . The dashed circle indicates the predicted maximal distance that a fluid parcel can travel when ejected from the source. The source is indicated by a green filled circle, and the sink is indicated by a red filled circle.

on the ground is around 1 m–2 m.^{56–58} These studies led to the Centers for Disease Control and Prevention (CDC)⁶² and World Health Organization (WHO)⁶³ social distancing guidelines. Nonetheless, the complex physics involved, which includes knowledge of the particle size distribution, their speed of evaporation, the viral charge of droplets of different size, the diffusivity of the virus-laden particles, etc., makes it difficult to assess what is the effective dispersion of the virus-laden fluid particles into the environment once ejected. It was found that the largest droplets generated by sneezing can reach a distance as far as 8 m,^{2,3,57} while aerosol dispersion is highly dependent on the temperature, humidity, and air currents. For these reasons, this paper does not aim to provide definitive measures for the aerosol displacements but contributes to building a body of evidence around this complex question.

B. Predicted droplet dispersion

Currently, there is a large amount of disagreement in the reported spectra of droplet sizes in respiratory events.² The analysis is complicated by various factors including the evaporation of the droplets as they travel from the source, which, in turn, is influenced by ambient humidity and temperature. Recent mathematical modeling of droplet emission during talking have categorized droplets into one of the three groups:⁵⁴ small ($<75 \mu\text{m}$), intermediate ($75 \mu\text{m}$ – $400 \mu\text{m}$), and large ($>400 \mu\text{m}$). Small droplets approximately follow the air and can travel a great distance by weakly feeling the effects of gravity. Large droplets can also travel a large distance due to their inertia. However, the intermediate-sized droplets feel strongly both gravity and drag, and their trajectory is a complex interaction of

TABLE I. Physical quantities for dispersion of droplets.

Quantity	Description	Value	Units
U'	Jet velocity (quiet) ^a	0.55	m s^{-1}
	Jet velocity (heavy) ^a	4.97	m s^{-1}
α	Jet angle (direction) ^a	-5.8	deg
β	Jet angle (spread) ^a	29.2	deg
ρ'_{air}	Density of air	1.149	kg m^{-3}
ρ'_{drop}	Density of droplet	1000	kg m^{-3}
ν'_{air}	Viscosity of air	16.36×10^{-6}	$\text{m}^2 \text{s}^{-1}$
Q'_1	Volume influx (quiet) ^a	23.8	l min^{-1}
	Volume influx (heavy) ^a	133	l min^{-1}
Q'_2	Volume outflux	0	l min^{-1}
$ x'_0 $	Characteristic length ^b	0.5	m

^aParameters taken from previous experimental studies.^{66,67}

^bTaken from wind tunnel experiments.⁵⁵

these effects. Similar trends were observed in computational fluid dynamics simulations of previous authors.⁶⁵

In this section, we examine the problem from a much simplified perspective: we ignore evaporation entirely. We model the situation

as a point source emitting droplets of various sizes in the presence of gravitational forces and compute the maximum horizontal distance traveled by these droplets. In this case, $Q'_2 = 0 \text{ l min}^{-1}$, and other quantities such as jet speed, direction, and spread are taken from recent experimental studies of the authors:⁶⁶ these quantities are summarized in Table I.

We find that for both heavy and quiet breathing, the maximum distance traveled by droplets L' (and the corresponding flight time τ') depends strongly on the droplet diameter (see Fig. 5). As expected, small droplets can travel many meters; however, we see that there is an intermediate range of droplet diameters where the horizontal distance is minimized. For quiet breathing, this minimum occurs between $69 \mu\text{m} < d < 77 \mu\text{m}$, while for heavy breathing, this minimum occurs between $50 \mu\text{m} < d < 55 \mu\text{m}$. This multi-modal behavior is reminiscent of that in previous experimental studies that measured the size distributions of droplets in various respiratory events such as talking and coughing^{54,55} and sneezing.⁴³ The multi-modal behavior observed in experiments is attributed to the different generation modes: bronchiolar, laryngeal, and oral. In our simplified model, we do not have any assumption on the biological origin of the droplet: the existence of the minimum is a characteristic of the droplets themselves and cannot be used as an indicator of the underlying droplet size distribution. The time it takes τ' decreases monotonically with increasing droplet diameter, as shown in Figs. 5(b) and 5(c).

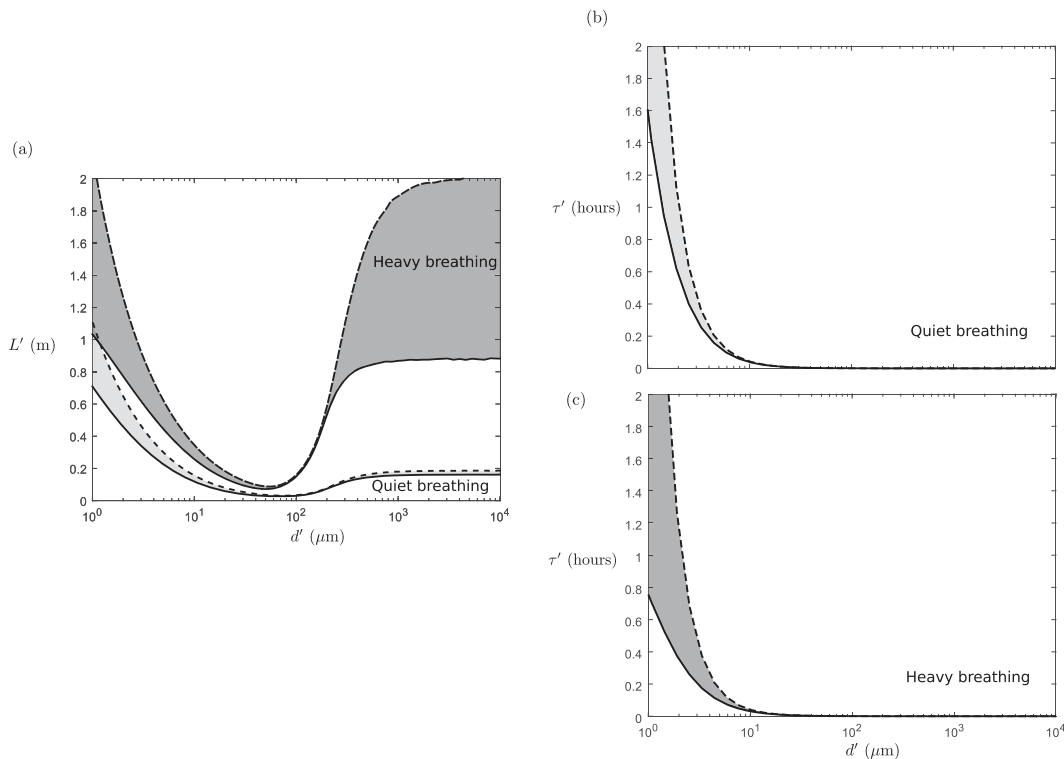


FIG. 5. (a) The maximum distance (L') traveled for droplets of various diameters (d') with quiet (light gray) and heavy (dark gray) breathing. [(b) and (c)] The total duration of travel τ' corresponding to the value of L' shown in (a) for quiet breathing (b) and heavy breathing (c). The dashed curve corresponds to trajectories with the ejection angle equal to $\alpha + \beta/2$, while the solid curve corresponds to trajectories with the ejection angle equal to $\alpha - \beta/2$ in Table I.

In order to unpick the physics, observe that the drag force scales with the diameter of the droplet, but the weight of the droplet scales with the diameter cubed; hence, for large droplets, the drag force is negligible in comparison with the inertia of the droplet. As shown before, the droplets are slowed down exponentially in the horizontal direction and are accelerated in the vertical direction by gravity, giving the maximum horizontal range of the droplet (when nominally $Y = -1$),

$$X = (St/R) \left(1 - \exp \left[-(R/St) \sqrt{\frac{2}{(1 - \frac{3}{2}R)|g|}} \right] \right). \quad (17)$$

For large droplets ($St \gg R$), we can then estimate that the maximum distance $L = L'/|\mathbf{x}'_0|$ is

$$L \approx \sqrt{\frac{2}{(1 - \frac{3}{2}R)|g|}}, \quad (18)$$

meaning that the trajectories are ballistic, and we expect that, for $St \gg R$, the maximum distance becomes independent of St , in agreement with the observation that large droplets' trajectories are independent of the surrounding flow.^{2,57,58}

For small droplets $St \ll R$, the drag decreases linearly with decreasing droplet diameter, but the weight rapidly decreases cubically with decreasing diameter. Hence, small droplets follow the air-flow faithfully with little influence from gravity. Such droplets can get great distances before falling, as shown in the left-hand side of Fig. 5(a).

In the case of small droplets, the horizontal component of the droplet's trajectory follows the airflow like a tracer, and the droplet falls at its Stokesian settling velocity. Upon inspection, we find that the maximum horizontal distance L (when nominally $Y = -1$) tends to the following asymptote as $St \rightarrow 0$:

$$L = \left(\frac{2 A \Lambda}{(1 - \frac{3}{2}R)|g|} \right)^{1/3}. \quad (19)$$

We can therefore estimate that droplets for which $L > 1$ or, equivalently,

$$St < \frac{2R\Lambda}{(1 - \frac{3}{2}R)|g|} \quad (20)$$

(i.e., the droplets travel farther in the horizontal direction than the vertical direction) weakly feel gravity.

In between these two extreme cases, the drag force on the droplet is the same order of magnitude as the gravitational force. By balancing these two effects, we can approximate the upper bound of St where the droplets become ballistic,

$$St < \frac{R}{(1 - \frac{3}{2}R)|g|}. \quad (21)$$

Such droplets are not light enough to get carried any great distance by the ambient airflow but do not have large enough inertia to become ballistic.

Hence, we have the following designations:

- (I) small droplets with St satisfying $St < \frac{2R\Lambda}{(1 - \frac{3}{2}R)|g|}$, which act like fluid tracers;
- (II) intermediate-sized droplets with $\frac{2R\Lambda}{(1 - \frac{3}{2}R)|g|} < St < \frac{R}{(1 - \frac{3}{2}R)|g|}$; and
- (III) large droplets with $St > \frac{R}{(1 - \frac{3}{2}R)|g|}$, which adopt ballistic trajectories.

This is illustrated in Fig. 6, where the black curves are the numerical solutions to quiet (a) and heavy (b) breathing at zero direction and spread angle⁶⁶ and the red dashed curves indicate the expressions in (18) for large St and (19) for small St . The black vertical lines indicate the distinction between small and intermediate-sized [see 20] and intermediate-sized and large droplets [see 21].

Reverting to dimensional quantities, we have the following range of intermediate-sized droplets:

$$\sqrt{\frac{9v'_{air}Q'_1\rho'_{air}}{\pi g'|\mathbf{x}'_0|^2(\rho'_{drop} - \rho'_{air})}} < d' < 2\sqrt{\frac{9v'_{air}\rho'_{air}U'}{2g'(\rho'_{drop} - \rho'_{air})}}. \quad (22)$$

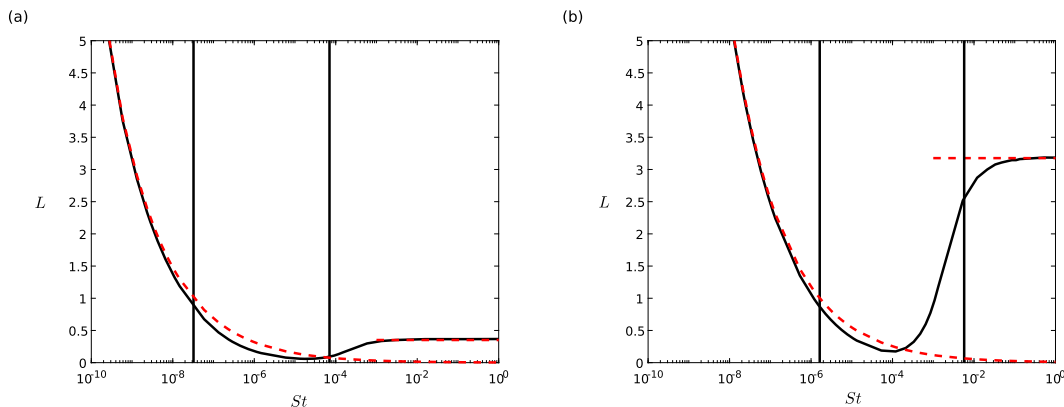


FIG. 6. The maximum distance (L) traveled for droplets of various St with quiet breathing (a) and heavy breathing (b). The vertical solid lines indicate the distinction between small and intermediate-sized [from (20)] and from intermediate-sized to large [from (21)]. The red dashed curves indicate the small- St (19) and large- St (18) limits.

TABLE II. Physical quantities for extraction.

Quantity	Description	Value	Units
U'	Breath jet velocity	1	m s^{-1}
ρ'_{air}	Density of air	1.149	kg m^{-3}
ρ'_{drop}	Density of droplet	1000	kg m^{-3}
ν'_{air}	Viscosity of air	16.36×10^{-6}	$\text{m}^2 \text{s}^{-1}$
Q'_1	Volume influx	6.5	l min^{-1}
Q'_2	Volume outflux	2832	l min^{-1}
$ \mathbf{x}'_0 $	Characteristic length ^a	0.2	m

^aThe characteristic length is chosen to be the source–sink distance.

Plugging in the numbers from Table I, we have the approximate range

$$3 \mu\text{m} < d' < 138 \mu\text{m} \quad (23)$$

for quiet breathing and

$$7 \mu\text{m} < d' < 414 \mu\text{m}, \quad (24)$$

for heavy breathing. Our upper bound is in good agreement with previous categorizations of droplets,⁶⁴ although our lower bound seems to be smaller than those found by previous authors.

C. The effectiveness of extraction on droplets

Consider a person breathing air of density $\rho'_{\text{air}} = 1.149 \text{ kg m}^{-3}$ and kinematic viscosity $\nu'_{\text{air}} = 16.36 \times 10^{-6} \text{ m}^2 \text{ s}^{-1}$ containing water droplets of density $\rho'_{\text{drop}} = 1000 \text{ kg m}^{-3}$. In human respiration,^{39,45} the exhaled droplets have diameters $d' = 2a'$ in the range of $0.5 \mu\text{m}$ – $2000 \mu\text{m}$. For a human breathing at rest, their average volume flux is in the range $Q'_1 = 5 \text{ l min}^{-1}$ – 8 l min^{-1} : these values of flow rate are similar to those in previous studies,⁶⁸ which reports 13 l min^{-1}

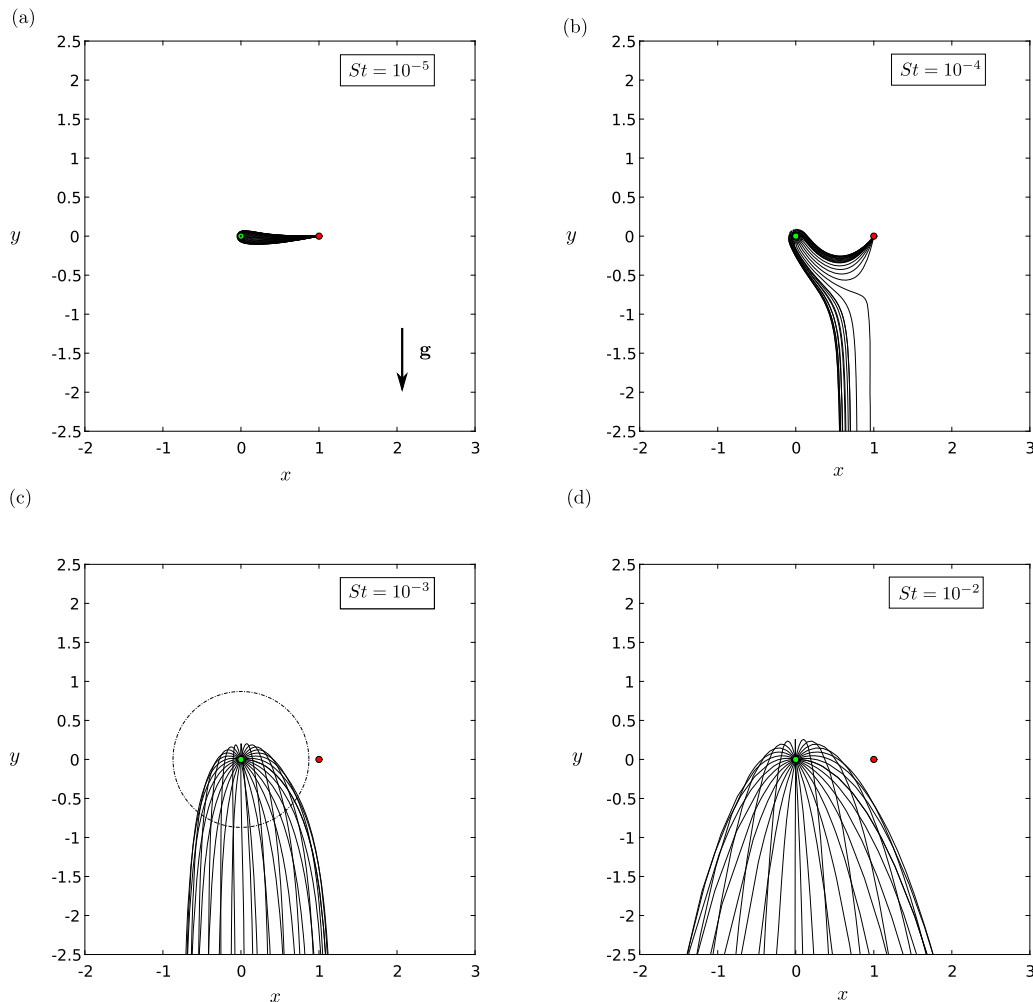


FIG. 7. The trajectories $\mathbf{X}(t)$ in the xy -plane with a background source–sink pair with strength ratio $\gamma = 436$ and for various Stokes numbers St : (a) $St = 10^{-5}$, (b) $St = 10^{-4}$, (c) $St = 10^{-3}$, and (d) $St = 10^{-2}$. In these plots, $R = 0.00115$, $\Lambda = 0.00022$, and $|\mathbf{g}| = 1.96$. The dashed-dotted circle indicates the maximal distance predicted by the inertia–drag balance. The source is indicated by a green filled circle, and the sink is indicated by a red filled circle.

for breathing, and the typical speed of a jet in normal breathing conditions is of the order of $U' = 1 \text{ m s}^{-1}$. In violent respiratory events, such as sneezing or coughing, these values could be significantly higher.² Finally, the extraction unit is located a distance of $|\mathbf{x}'_0| = 0.2 \text{ m}$ from the person. These quantities are summarized in Table II.

Based on these numbers, the non-dimensional parameters that govern the trajectory of the droplet are determined to be $R = 0.00115$, $Re = 12, 225$, $\Lambda = 0.00022$, and $|\mathbf{g}| = 1.96$, and the Stokes number ranges approximately from 10^{-9} to 10^{-1} . The parameter γ relates the flux of the extraction unit to the flux of a human's breath, and its effect will be examined. In particular, if we suppose that the envisaged extraction unit has a volume flux approximately equal to that of a standard vacuum cleaner (2832 l min^{-1}), then we can approximate that $\gamma \approx 436$. In Fig. 7, we show the efficacy of such extraction for a range of St . Extraction is very effective at low St ; however, for $St > 8.5 \times 10^{-5}$, such extraction is ineffective. This upper bound of the Stokes number corresponds to water droplets of diameter $71 \mu\text{m}$. Droplets larger than this will not be collected by extraction. In the droplet classification of Sec. IV B, the effective range of extraction corresponds to non-ballistic droplets.

V. DISCUSSION AND CONCLUSION

In this paper, we have presented a simplified mathematical model for droplet dispersion from a source and in the presence an aerosol extractor. In the absence of gravity, and for $St \ll R$, droplets behave as ideal tracers, and the maximum distance that they can travel before being extracted is a function of γ only. In this case, there are two (source, and sink if $\gamma = 1$) or three (source, sink, and saddle if $\gamma > 1$) fixed points. The fixed points in this study are colinear, and the position of the saddle depends on γ alone, for any given distance between the source and sink. For moderate St , the droplets' inertia carry them far away from the source until they are slowed down by drag forces and pulled into the sink. In this case, the maximum distance that the droplets can travel is given by R/St .

When gravity effects are taken into account, the saddle point for $St \ll R$ is no longer colinear but moves on an arc, clockwise about the source, and a fourth fixed point (saddle) emerges approximately below the sink fixed point. For fixed γ , this fixed point moves closer to the source as the magnitude of gravity is increased. In this case, there is a set of trajectories that are pulled away from the sink by gravity. For moderate St , gravity plays an increasingly important role, and there is a critical value of gravity that pulls all trajectories vertically downwards away from the source. For yet larger St , the trajectories adopt a ballistic trajectory, with even those that travel close to the sink not being pulled in.

COVID-19 has brought increased awareness of the risks of aerosol generating procedures (AGPs) across all fields of medicine, highlighting the need for a deeper understanding of droplet dispersion and categorization during respiration and AGPs. Clinicians recognize that our historical approaches to protection during AGPs are no longer adequate and that many additional precautions are necessary. In order to develop the most effective solutions, a critical first step is understanding the behavior of droplets generated during

AGPs. This paper allows us to predict this behavior and inform our understanding of "at risk" zones in the vicinity of an AGP. In particular, we performed simulations relevant to human respiration, as well as simulations to inform the development of an aerosol extractor for use in clinical settings. These simulations can help to guide recommendations on maximum safe distances between the source and sink.

Additionally, these models provide a better understanding of the behavior of individual droplets of various sizes, which may be present in a wide range of aerosols contaminated with viruses or other pathogens. This may help clinicians to make better informed decisions regarding safety while performing AGPs and in their choices of the type of PPE they wear. Finally, these models provide a basis on which aerosol and droplet contamination from a wide range of surgical, medical, dental, and veterinary AGPs can be modeled while taking into account airflows in confined clinical spaces. In this case, we found that, for $St \leq 8.5 \times 10^{-5}$, all of the aerosol is extracted and that gravity has a minimal effect; this St corresponds to droplets with approximate diameter equal to 0.07 mm . Droplets larger than this are affected by gravity, and for $St = 10^{-2}$, corresponding to droplets equal to 0.78 mm , none of the droplets are extracted. Such large droplets would be typically captured by personal protective equipment (PPE), such as FFP1 masks that have pore sizes typically smaller than $1 \mu\text{m}$.

We determined the maximum range of droplets ejected from the source in the absence of a sink and found that the range is minimized for intermediate-sized droplets. We find that, in human respiration, this pertains to droplets within the observed range of the ejected droplets. This could have implications for the interpretation for data obtained from experiments on biological subjects, in particular, those that attribute observed bi- and tri-modal droplet dispersion to biological functions. Our studies suggest that the bi-modal nature of the curve is a function of the droplet's Stokes number and not necessarily linked to a specific biological function.

In our model, we neglected the Basset history term in the Maxey–Riley equation. The Basset history term is of significant importance for bubbly flows, where it can account for a quarter of the instantaneous force on a bubble.¹⁴ Generally speaking, for $R \ll 2/3$, this term can be safely ignored for small and intermediate-sized droplets. Recent studies have also shown that neglecting it in the modeling of raindrop growth leads to a substantial overestimate of the growth rate of the droplet. Hence, for the solutions that become ballistic, we expect that such trajectories would be influenced by the Basset history term that should be included. To do this efficiently, there is a very promising method developed recently.¹⁵ Since this is not the focus of our study (such droplets can be captured by other forms of PPE), we do not perform such a study here.

If the aerosol route of transmission is confirmed to be important by the World Health Organization,^{20,69} we will need to reconsider guidelines on social distancing, ventilation systems, and shared spaces. To ensure that we put in place the correct mitigating measures, for example, face coverings, we need to have a better understanding of the different droplet behaviors and their different dispersion mechanisms depending on their size. This paper contributes to this debate by providing a new framework for categorizing droplets depending on their dispersion mechanism.

ACKNOWLEDGMENTS

O.J.A. acknowledges the support of the Commonwealth Scholarship Commission. F.V.M. acknowledges the support of Caledonian Heritable Limited.

DATA AVAILABILITY

The data that support the findings of this study are available from the corresponding author upon reasonable request.

REFERENCES

- ¹F. J. Beron-Vera, M. J. Olascoaga, and P. Miron, "Building a Maxey-Riley framework for surface ocean inertial particle dynamics," *Phys. Fluids* **31**, 096602 (2019).
- ²L. Bourouiba, E. Dehandschoewercker, and J. W. M. Bush, "Violent expiratory events: On coughing and sneezing," *J. Fluid Mech.* **745**, 537–563 (2014).
- ³L. Bourouiba, "Turbulent gas clouds and respiratory pathogen emissions: Potential implications for reducing transmission of COVID-19," *J. Am. Med. Assoc.* **323**, 1837–1838 (2020).
- ⁴S. Verma, M. Dhanak, and J. Frankenfield, "Visualizing the effectiveness of face masks in obstructing respiratory jets," *Phys. Fluids* **32**, 061708 (2020).
- ⁵M. R. Maxey and J. J. Riley, "Equation of motion for a small rigid sphere in a nonuniform flow," *Phys. Fluids* **26**, 883–889 (1983).
- ⁶M. Farazmand and G. Haller, "The Maxey–Riley equation: Existence, uniqueness and regularity of solutions," *Nonlinear Anal.: Real World Appl.* **22**, 98–106 (2015).
- ⁷M. R. Maxey, "The motion of small spherical particles in a cellular flow field," *Phys. Fluids* **30**, 1915–1928 (1987).
- ⁸J. H. Costello and S. P. Colin, "Morphology, fluid motion and predation by the scyphomedusa *Aurelia aurita*," *Mar. Biol.* **121**, 327–334 (1994).
- ⁹J. Peng and J. O. Dabiri, "Transport of inertial particles by Lagrangian coherent structures: Application to predator-prey interaction in jellyfish feeding," *J. Fluid Mech.* **623**, 75–84 (2009).
- ¹⁰O. A. Druzhinin, "Concentration waves and flow modification in a particle-laden circular vortex," *Phys. Fluids* **6**, 3276–3284 (1994).
- ¹¹N. Raju and E. Meiburg, "Dynamics of small, spherical particles in vortical and stagnation point flow fields," *Phys. Fluids* **9**, 299–314 (1997).
- ¹²S. Ravichandran and R. Govindarajan, "Caustics and clustering in the vicinity of a vortex," *Phys. Fluids* **27**, 033305 (2015).
- ¹³S. Ravichandran, R. Govindarajan, and R. Govindarajan, "Vortex-dipole collapse induced by droplet inertia and phase change," *J. Fluid Mech.* **832**, 745–776 (2017).
- ¹⁴E. E. Michaelides, "Review—The transient equation of motion for particles, bubbles, and droplets," *J. Fluids Eng.* **119**, 233–247 (1997).
- ¹⁵S. G. Prasath, V. Vasanth, and R. Govindarajan, "Accurate solution method for the Maxey–Riley equation, and the effects of Basset history," *J. Fluid Mech.* **868**, 428–460 (2019).
- ¹⁶G. P. Langlois, M. Farazmand, and G. Haller, "Asymptotic dynamics of inertial particles with memory," *J. Nonlinear Sci.* **25**, 1225–1255 (2015).
- ¹⁷G. K. Batchelor, *An Introduction to Fluid Dynamics* (Cambridge University Press, 2000).
- ¹⁸T. Dbouk and D. Drikakis, "On coughing and airborne droplet transmission to humans," *Phys. Fluids* **32**, 053310 (2020).
- ¹⁹B. Rosa, H. Parishani, O. Ayala, and L.-P. Wang, "Settling velocity of small inertial particles in homogeneous isotropic turbulence from high-resolution DNS," *Int. J. Multiphase Flow* **83**, 217–231 (2016).
- ²⁰G. Busco, S. R. Yang, J. Seo, and Y. A. Hassan, "Sneezing and asymptomatic virus transmission," *Phys. Fluids* **32**, 073309 (2020).
- ²¹L. F. Shampine and M. W. Reichelt, "The MATLAB ODE suite," *SIAM J. Sci. Comput.* **18**(1), 1–22 (1997).
- ²²J. Xi, J. Kim, and X. A. Si, "Effects of nostril orientation on airflow dynamics, heat exchange, and particle depositions in human noses," *Eur. J. Mech.: B/Fluids* **55**, 215–228 (2016).
- ²³R. Mittal, R. Ni, and J.-H. Seo, "The flow physics of COVID-19," *J. Fluid Mech.* **894**, F2 (2020).
- ²⁴M. Nicas, W. W. Nazaroff, and A. Hubbard, "Toward understanding the risk of secondary airborne infection: Emission of respirable pathogens," *J. Occup. Environ. Hyg.* **2**, 143–154 (2005).
- ²⁵R. Tellier, "Review of aerosol transmission of influenza A virus," *Emerging Infect. Dis.* **12**, 1657–1662 (2006).
- ²⁶N. van Doremalen, T. Bushmaker, D. H. Morris, M. G. Holbrook, A. Gamble, B. N. Williamson, A. Tamin, J. L. Harcourt, N. J. Thornburg, S. I. Gerber, J. O. Lloyd-Smith, E. de Wit, and V. J. Munster, "Aerosol and surface stability of SARS-CoV-2 as compared with SARS-CoV-1," *N. Engl. J. Med.* **382**, 1564–1567 (2020).
- ²⁷R. M. Jones and L. M. Brosseau, "Aerosol transmission of infectious disease," *J. Occup. Environ. Med.* **57**, 501–508 (2015).
- ²⁸J.-M. Kim, Y.-S. Chung, H. J. Jo, N.-J. Lee, M. S. Kim, S. H. Woo, S. Park, J. W. Kim, H. M. Kim, and M.-G. Han, "Identification of coronavirus isolated from a patient in Korea with COVID-19," *Osong Public Health Res. Perspect.* **11**, 3–7 (2020).
- ²⁹Y. Liu, Z. Ning, Y. Chen, M. Guo, Y. Liu, N. K. Gali, L. Sun, Y. Duan, J. Cai, D. Westerdahl, X. Liu, K. Xu, K.-f. Ho, H. Kan, Q. Fu, and K. Lan, "Aerodynamic analysis of SARS-CoV-2 in two Wuhan hospitals," *Nature* **582**, 557–560 (2020).
- ³⁰N. H. L. Leung, D. K. W. Chu, E. Y. C. Shiu, K.-H. Chan, J. J. McDevitt, B. J. P. Hau, H.-L. Yen, Y. Li, D. K. M. Ip, J. S. M. Peiris, W.-H. Seto, G. M. Leung, D. K. Milton, and B. J. Cowling, "Respiratory virus shedding in exhaled breath and efficacy of face masks," *Nat. Med.* **26**, 676–680 (2020).
- ³¹R. Zhang, Y. Li, A. L. Zhang, Y. Wang, and M. J. Molina, "Identifying airborne transmission as the dominant route for the spread of COVID-19," *Proc. Natl. Acad. Sci. U. S. A.* **117**, 14857–14863 (2020).
- ³²D. K. Milton, M. P. Fabian, B. J. Cowling, M. L. Grantham, and J. J. McDevitt, "Influenza virus aerosols in human exhaled breath: Particle size, culturability, and effect of surgical masks," *PLoS Pathog.* **9**, e1003205 (2013).
- ³³W. G. Lindsley, J. D. Noti, F. M. Blachere, R. E. Thewlis, S. B. Martin, S. Othumpangat, B. Noorbakhsh, W. T. Goldsmith, A. Vishnu, J. E. Palmer, K. E. Clark, and D. H. Beezhold, "Viable influenza A virus in airborne particles from human coughs," *J. Occup. Environ. Hyg.* **12**, 107–113 (2015).
- ³⁴W. J. Fokkens and R. A. Scheeren, "Upper airway defence mechanisms," *Paediatr. Respir. Rev.* **1**, 336–341 (2000).
- ³⁵J. Atkinson and World Health Organization, *Natural Ventilation for Infection Control in Health-Care Settings* (World Health Organization, 2009), p. 106.
- ³⁶G. Zayas, M. C. Chiang, E. Wong, F. MacDonald, C. F. Lange, A. Senthilvelan, and M. King, "Cough aerosol in healthy participants: Fundamental knowledge to optimize droplet-spread infectious respiratory disease management," *BMC Pulm. Med.* **12**, 11 (2012).
- ³⁷J. Yan, M. Grantham, J. Pantelic, P. J. Bueno de Mesquita, B. Albert, F. Liu, S. Ehrman, and D. K. Milton, "Infectious virus in exhaled breath of symptomatic seasonal influenza cases from a college community," *Proc. Natl. Acad. Sci. U. S. A.* **115**, 1081–1086 (2018).
- ³⁸W. G. Lindsley, F. M. Blachere, R. E. Thewlis, A. Vishnu, K. A. Davis, G. Cao, J. E. Palmer, K. E. Clark, M. A. Fisher, R. Khakoo, and D. H. Beezhold, "Measurements of airborne influenza virus in aerosol particles from human coughs," *PLoS One* **5**, e15100 (2010).
- ³⁹S. Asadi, A. S. Wexler, C. D. Cappa, S. Barreda, N. M. Bouvier, and W. D. Ristenpart, "Aerosol emission and superemission during human speech increase with voice loudness," *Sci. Rep.* **9**, 2348 (2019).
- ⁴⁰J. W. Tang, A. D. Nicolle, C. A. Klettner, J. Pantelic, L. Wang, A. B. Suhaimi, A. Y. L. Tan, G. W. X. Ong, R. Su, C. Sekhar, D. D. W. Cheong, and K. W. Tham, "Airflow dynamics of human jets: Sneezing and breathing - Potential sources of infectious aerosols," *PLoS One* **8**, e59970 (2013).
- ⁴¹J. Fiegel, R. Clarke, and D. A. Edwards, "Airborne infectious disease and the suppression of pulmonary bioaerosols," *Drug Discovery Today* **11**, 51–57 (2006).
- ⁴²M. P. Atkinson and L. M. Wein, "Quantifying the routes of transmission for pandemic influenza," *Bull. Math. Biol.* **70**, 820–867 (2008).

- ⁴³Z. Y. Han, W. G. Weng, and Q. Y. Huang, “Characterizations of particle size distribution of the droplets exhaled by sneeze,” *J. R. Soc., Interface* **10**, 20130560 (2013).
- ⁴⁴J. P. Duguid, “The numbers and the sites of origin of the droplets expelled during expiratory activities,” *Edinburgh Med. J.* **52**, 385–401 (1945).
- ⁴⁵J. P. Duguid, “The size and the duration of air-carriage of respiratory droplets and droplet-nuclei,” *Epidemiol. Infect.* **44**, 471–479 (1946).
- ⁴⁶R. G. Loudon and R. M. Roberts, “Relation between the airborne diameters of respiratory droplets and the diameter of the stains left after recovery,” *Nature* **213**, 95–96 (1967).
- ⁴⁷R. S. Papineni and F. S. Rosenthal, “The size distribution of droplets in the exhaled breath of healthy human subjects,” *J. Aerosol Med.* **10**, 105–116 (1997).
- ⁴⁸L. Morawska, “Droplet fate in indoor environments, or can we prevent the spread of infection?,” *Indoor Air* **16**, 335–347 (2006).
- ⁴⁹L. Morawska, G. R. Johnson, Z. D. Ristovski, M. Hargreaves, K. Mengersen, S. Corbett, C. Y. H. Chao, Y. Li, and D. Katoshevski, “Size distribution and sites of origin of droplets expelled from the human respiratory tract during expiratory activities,” *J. Aerosol Sci.* **40**, 256–269 (2009).
- ⁵⁰S. Yang, G. W. M. Lee, C.-M. Chen, C.-C. Wu, and K.-P. Yu, “The size and concentration of droplets generated by coughing in human subjects,” *J. Aerosol Med.* **20**, 484–494 (2007).
- ⁵¹C. Y. H. Chao, M. P. Wan, L. Morawska, G. R. Johnson, Z. D. Ristovski, M. Hargreaves, K. Mengersen, S. Corbett, Y. Li, X. Xie, and D. Katoshevski, “Characterization of expiration air jets and droplet size distributions immediately at the mouth opening,” *J. Aerosol Sci.* **40**, 122–133 (2009).
- ⁵²B. E. Scharfman, A. H. Techet, J. W. M. Bush, and L. Bourouiba, “Visualization of sneeze ejecta: Steps of fluid fragmentation leading to respiratory droplets,” *Exp. Fluids* **57**, 24 (2016).
- ⁵³V. Stadnytskyi, C. E. Bax, A. Bax, and P. Anfinrud, “The airborne lifetime of small speech droplets and their potential importance in SARS-CoV-2 transmission,” *Proc. Natl. Acad. Sci. U. S. A.* **117**, 11875–11877 (2020).
- ⁵⁴X. Xie, Y. Li, H. Sun, and L. Liu, “Exhaled droplets due to talking and coughing,” *J. R. Soc., Interface* **6**, S703–S714 (2009).
- ⁵⁵G. R. Johnson, L. Morawska, Z. D. Ristovski, M. Hargreaves, K. Mengersen, C. Y. H. Chao, M. P. Wan, Y. Li, X. Xie, D. Katoshevski, and S. Corbett, “Modality of human expired aerosol size distributions,” *J. Aerosol Sci.* **42**, 839–851 (2011).
- ⁵⁶W. F. Wells, “On air-borne infection study II: Droplets and droplet nuclei,” *Am. J. Epidemiol.* **20**, 611–618 (1934).
- ⁵⁷X. Xie, Y. Li, A. T. Y. Chwang, P. L. Ho, and W. H. Seto, “How far droplets can move in indoor environments—Revisiting the wells evaporation-falling curve,” *Indoor Air* **17**, 211–225 (2007).
- ⁵⁸J. Wei and Y. Li, “Enhanced spread of expiratory droplets by turbulence in a cough jet,” *Build. Environ.* **93**, 86–96 (2015).
- ⁵⁹B. R. Morton, G. I. Taylor, and J. S. Turner, “Turbulent gravitational convection from maintained and instantaneous sources,” *Proc. R. Soc. London, Ser. A* **234**, 1–23 (1956).
- ⁶⁰H. Holterman, “Kinetics and evaporation of water drops in air,” IMAG Report No. 2003-12, IMAG, 2003.
- ⁶¹A. K. Melikov and J. Kaczmarczyk, “Air movement and perceived air quality,” *Build. Environ.* **47**, 400–409 (2012).
- ⁶²CDC, Social distancing, 2020.
- ⁶³WHO, “Clinical management of severe acute respiratory infection (SARI) when COVID-19 disease is suspected,” Technical Report, World Health Organization, 2020.
- ⁶⁴W. Chen, N. Zhang, J. Wei, H.-L. Yen, and Y. Li, “Short-range airborne route dominates exposure of respiratory infection during close contact,” *Build. Environ.* **176**, 106859 (2020).
- ⁶⁵S. Zhu, S. Kato, and J.-H. Yang, “Study on transport characteristics of saliva droplets produced by coughing in a calm indoor environment,” *Build. Environ.* **41**, 1691–1702 (2006).
- ⁶⁶I. Viola, B. Peterson, G. Pisetta, G. Pavar, H. Akhtar, F. Menoloascina, E. Mangano, K. Dunn, R. Gabl, A. Nila *et al.*, “Face coverings, aerosol dispersion and mitigation of virus transmission risk,” [arXiv:2005.10720](https://arxiv.org/abs/2005.10720) (2020).
- ⁶⁷I. M. Viola, B. Peterson, G. Pisetta, G. Pavar, H. Akhtar, F. Menoloascina, E. Mangano, A. Nila, E. Molinari, C. Cummins *et al.*, *Aerosol Dispersion and Mitigation of Infection Risk - Dataset 1 of 4 [dataset]*, University of Edinburgh, School of Engineering, Institute for Energy Systems, 2020.
- ⁶⁸J. K. Gupta, C.-H. Lin, and Q. Chen, “Characterizing exhaled airflow from breathing and talking,” *Indoor Air* **20**, 31–39 (2010).
- ⁶⁹World Health Organization, Novel coronavirus (2019-ncov): Situation report, 19, Technical documents, 2020.